

Article

Defect-Rich Nickel Nanoparticles Supported on SiC Derived from Silica Fume with Enhanced Catalytic Performance for CO Methanation

Qi Song¹, Xingwu Zhai^{1,2}, Feng Yu^{1,*} , Jiangbing Li¹, Xin Ren¹, Haiyang Zhang¹ , Mingyuan Zhu¹, Bin Dai¹, Guixian Ge^{2,*} and Jinli Zhang^{1,*}

¹ Key Laboratory for Green Processing of Chemical Engineering of Xinjiang Bingtuan, School of Chemistry and Chemical Engineering, Shihezi University, Shihezi 832003, China; ccsongqi@yeah.net (Q.S.); zwxw1725910806@163.com (X.Z.); ljbin@shzu.edu.cn (J.L.); renxin_shzu@163.com (X.R.); zhy198722@163.com (H.Z.); zhumin yuan@shzu.edu.cn (M.Z.); db_tea@shzu.edu.cn (B.D.)

² Key Laboratory of Ecophysics and Department of Physics, College of Science, Shihezi University, Xinjiang 832003, China

* Correspondence: yufeng05@mail.ipc.ac.cn (F.Y.); geguixian@126.com (G.G.); zhangjinli@tju.edu.cn (J.Z.); Tel.: +86-993-205-7272 (F.Y. & G.G. & J.Z.); Fax: +86-993-205-7270 (F.Y. & G.G. & J.Z.)

Received: 23 January 2019; Accepted: 20 March 2019; Published: 24 March 2019



Abstract: With the increased demands of environmental protection, recycling/utilization of industrial byproducts has attracted much attention from both industry and academic communities. In this work, silicon carbide (SiC) was successfully synthesized from industrial waste silica fume (SF) during metallic silicon production. Following this, Ni nanoparticles with many defects were supported on the as-obtained SiC by conventional impregnation method. The results showed that defect-rich Ni nanoparticles were dispersed onto the surface of SiC. The as-obtained Ni/SF-SiC exhibited an enhanced metal-support interaction between Ni and SiC. Furthermore, the density functional theory (DFT) calculations showed that the H₂ and CO adsorption energy on Ni vacancy (V_{Ni}) sites of Ni/SF-SiC were 1.84 and 4.88 eV, respectively. Finally, the Ni/SF-SiC performed high catalytic activity with CO conversion of 99.1% and CH₄ selectivity of 85.7% at 350 °C, 0.1 MPa and a gas hourly space velocity (GHSV) of 18,000 mL·g⁻¹·h⁻¹. Moreover, Ni/SF-SiC processed good catalytic stability in the 50 h continuous reaction.

Keywords: defect-rich catalyst; silicon carbide; silica fume; synthetic natural gas; carbon monoxide methanation

1. Introduction

Metallic silicon is also known as industrial silicon or crystalline silicon and is usually produced by reducing silicon dioxide from carbon in an electric furnace. It is mainly used as an additive for non-ferrous alloys or as a raw material for the production of semiconductor silicon and silicone. The amount of metallic silicon production capacity in China was 7.5 million tons in 2018. With growing demand for metallic silicon, the related industries have been burgeoning. It is inevitable that a large amount of silica fume is derived from metallic production (about 0.3 tons of silicon fume/ton of products). However, handling the problems of silica fume properly is not easy or smooth during the production. There is a large quantity of silica fume deserted in industrial disposal, which not only brings about resource wastage, but also results in serious pollution from the dust and powder [1,2].

Silica fume has excellent properties of pozzolanic, which is mainly used in concrete and refractory materials [3]. Recently, silica fume was widely used as support for the reaction of dry reforming of methane [4], or as silica source of producing mesoporous silicate materials (MCM-41, SAB-15, zeolite

SSZ-13, etc.) and to synthesize SiC/Si₃N₄ powder [5–7]. A porous silicon nano-cluster was synthesized by using waste silica fume from the metallurgical grade silicon industry (MG-Si). This material was used in lithium ion batteries, showing excellent electrochemical properties [8]. However, further utilization of silica fume has seldom been realized, and therefore it is necessary to develop a new technique to produce materials beneficial to the economy and environment.

The present study concentrates on the synthesis of silicon carbide ceramic material, and then on successfully preparing a Ni/SF-SiC catalyst, using silica fume as the raw material. Considering that silica fume contains more than 97% of SiO₂ and a small amount of SiC, silica fume has naturally become an ideal raw material for SiC production, as well as for its associated decrease of production cost. In recent years, with increased demand on natural gas, and the aspiration to strengthen national energy security and increase energy efficiency, the production of synthetic natural gas (SNG) from coal or biomass has aroused widespread concern [9–13]. Being a good potential material, SiC has extensive applications in many fields, especially working in harsh environments as a support due to its excellent properties including high heat conductivity, thermal stability, mechanical strength, and chemical inertness [14–19]. SiC has been applied to various reactions, including methane reforming and combustion, Fischer–Tropsch synthesis, isomerization and dehydrogenation, among others [20,21]. Therefore, making full use of the waste generated during industrial production not only achieves the maximum use of resources, but also makes a great contribution to the protection of the environment. Additionally, a Ni/SF-SiC catalyst with metal defects is a promising approach to enhance the catalytic activity of methanation.

2. Results and Discussion

The reactivity of Ni/SF-SiO₂ and Ni/SF-SiC catalysts was tested at 250–550 °C at a GHSV 18,000 mL·g⁻¹·h⁻¹ and 0.1 MPa, as shown in Figure 1. With increasing test temperature, the catalytic performances of these catalysts were improved. There are some differences as the reaction temperature raised to 250 °C: The CH₄ selectivity of Ni/SF-SiC was 84.1%, while Ni/SF-SiO₂ was 0%. At 350 °C, the CO conversion of the catalyst Ni/SF-SiC achieved 99.1%, and the CO conversion of the catalyst Ni/SF-SiO₂ was only 89.8%. Furthermore, the CH₄ selectivity and yield for Ni/SF-SiC catalyst was 85.7% and 84.9% at 350 °C, respectively, but for Ni/SF-SiO₂ catalyst, the CH₄ selectivity and yield was only 75.0% and 67.4%, respectively. In addition, we researched the 50 h stability test for Ni/SF-SiO₂ and Ni/SF-SiC at 350 °C, and the results are presented in Figure 1c. The reactivity and stability of Ni/SF-SiC are much better than Ni/SF-SiO₂ [22]. When the temperature went beyond 400 °C, these catalysts decreased slightly in catalytic activity, because the catalyst Ni/SF-SiC was limited by thermodynamics in the strongly exothermic reaction. In a high temperature reaction, it is easy for the Ni/SF-SiO₂ catalyst to be sintered and carbon deposited, which results in the decrease of catalyst activity [23–25]. In Table 1, we compared the CO catalytic performances of different catalysts, and the catalyst Ni/SF-SiC exhibited excellent performance.

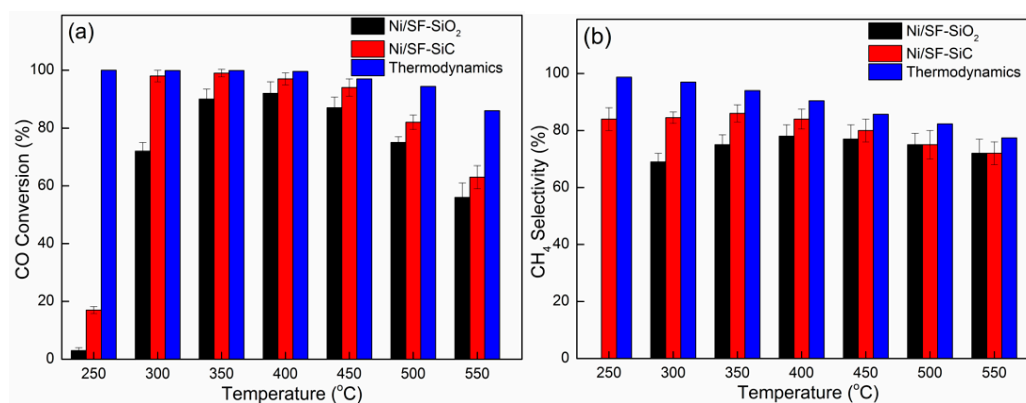


Figure 1. Cont.

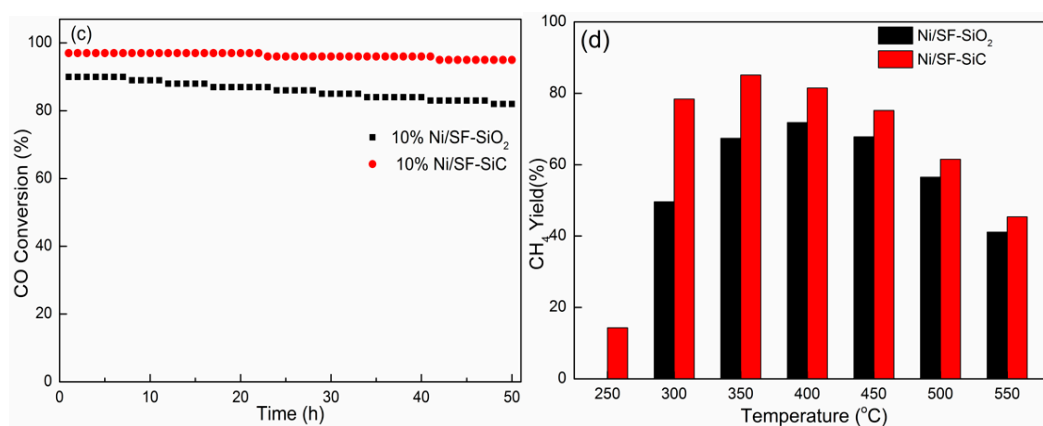


Figure 1. Catalytic performances of catalysts in CO methanation under different reaction temperatures at 0.1 MPa and GHSV of 18,000 mL·g⁻¹·h⁻¹: (a) CO Conversion, (b) CH₄ Selectivity and (d) CH₄ yield of Ni/SF-SiO₂ and Ni/SF-SiC; (c) long-time stability test of Ni/SF-SiO₂ and Ni/SF-SiC at 350 °C, 0.1 MPa and GHSV of 18000 mL·g⁻¹·h⁻¹.

The detailed information for components of the supports and catalysts were investigated by X-ray diffraction (XRD). In Figure 2, the diffraction peaks of SF-SiC and Ni/SF-SiC at 34.8°, 35.72°, 38.23°, 41.50°, 49.77°, 60.15°, 65.80°, 71.96°, 73.59° and 75.65° are related to distinct peaks of SiC (JCPDS 29-1131) [26]. In addition, SiC characteristic peaks at 2θ of 35.72°, 60.15° and 71.96° of the support, fresh and used Ni/SF-SiO₂, were also clearly observed. Furthermore, the diffraction peak at 21.98° was attached to SiO₂ (JCPDS 29-0085). For the above catalysts, the diffraction peaks at 44.50°, 51.84° and 76.37° belonged to face centered cubic Ni (JCPDS 04-0850) [27]. In the Ni/SF-SiC catalyst, the intensity of Ni diffraction peak was slightly weaker than the Ni/SF-SiC catalyst, revealing the higher dispersion of Ni species over the Ni/SF-SiC catalyst surfaces [28]. The mean size estimation of Ni crystallites is discussed by the Scherrer equation, and the results are shown in Table 2 [29,30]. Compared with the Ni/SF-SiO₂ catalyst, the crystallite size of Ni in the Ni/SF-SiC catalyst did not change before and after the reaction, which shows the Ni/SF-SiC catalysts possesses an excellent anti-sintering property. However, in the used Ni/SF-SiO₂ catalyst, the crystallite size of Ni particle was larger than the freshly reduced Ni/SF-SiO₂ catalyst; this phenomenon can be ascribed mainly to the aggregation of Ni species of Ni/SF-SiO₂, which further indicates that the Ni/SF-SiC catalyst has better anti-sintering and anti-aggregation properties than Ni/SF-SiO₂ catalyst [21].

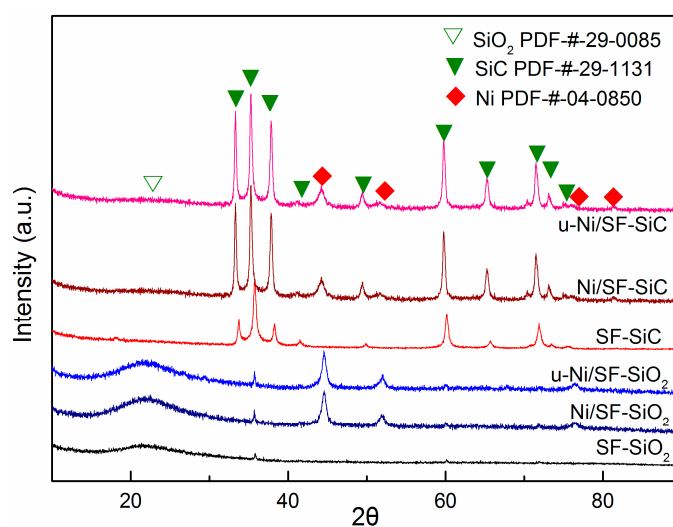


Figure 2. Wide-angle XRD patterns of the support and the catalysts SF-SiO₂, Ni/SF-SiO₂, u-Ni/SF-SiO₂, SF-SiC, Ni/SF-SiC, u-Ni/SF-SiC.

Table 1. The comparison of catalytic performance in different works.

Catalysts	Raw Material	Optimum Temperature (°C)	Pressure (MPa)	Space Velocity (mL·g ⁻¹ ·h ⁻¹)	CO Conversion (%)	CH ₄ Selectivity (%)	Space-Time Yield CH ₄ (mL·g ⁻¹ ·h ⁻¹)	Refs.
7%Ce-10%Ni/SiC	SiO ₂	600	1	60,000	95	85	41,182	[28]
10%Ni/VMT-SiO ₂	Vermiculite (VMT)	450	1.5	20,745	85.9	78	13,899	[31]
10%Ni/SiO ₂	SiO ₂	420	–	60,000	95.8	75.2	43,225	[29]
10%NiO/VMT-LDO	VMT-waste water	400	1.5	20,000	87.88	89.97	15,813	[9]
10%Ni/SBA-15(ET)	Tetraethylorthosilicate	400	0.3	15,000	100	–	–	[30]
10%NiO/Al ₂ O ₃	Al ₂ O ₃	350	0.1	120,000	91.2	75	82,080	[32]
10%Ni/SF-SiC	Waste silica fume	350	0.1	18,000	99.1	85.7	15,287	This work
20%NiO/Al ₂ O ₃ -SiC	SiO ₂	320	0.1	30,000	99	82	25,800	[21]

Table 2. Physical and chemical properties of the catalysts and supports.

Samples	S _{BET} (m ² /g) ¹	V _p (cm ³ /g) ²	V _p (cm ³ /g) ^{2*}	D _p (nm) ²	D _p (nm) ^{2*}	D _{Ni} (nm) ³	D _{Ni} (nm) ⁴
SF-SiO ₂	18.6	0.10	0.10	36.4	39.6	–	–
Ni/SF-SiO ₂	21.0	0.13	0.13	34.1	36.9	12.6	15.6
u-Ni/SF-SiO ₂	21.2	0.13	0.13	31.3	33.0	18.9	17.7
SF-SiC	45.2	0.20	0.20	19.9	19.1	–	–
Ni/SF-SiC	36.7	0.18	0.18	22.3	22.1	10.9	16.9
u-Ni/SF-SiC	42.2	0.18	0.18	21.3	20.9	12.3	16.9

¹ Surface area derived from the Brunauer–Ennett–Teller (BET) equation. ² Desorption average pore volume and pore diameter derived from Barret-Joyner-Halenda (BJH) method. ^{2*} Adsorption average pore volume and pore diameter derived from Barret-Joyner-Halenda (BJH) method. ³ Calculated according to equation $D_{Ni} = \sum Ni D_i^3 / \sum Ni D_i^2$ from HRTEM. ⁴ Estimated from the XRD diffraction peak ($2\theta = 44.6$) using the Scherrer equation as follows: $L = 0.9\lambda_{k\alpha 1} / B_{(2\theta)} \cos\theta_{max}$ where L denotes the average particle size, 0.9 is the value in radians when $B_{(2\theta)}$ is the full width at half maximum (FWHM) of the peak, $k\alpha 1$ is the wavelength of the X-ray radiation (0.15406 nm), and max is the angular position at the (1 1 1) peak maximum of Ni.

From the SEM and HRTEM images, the fine spherical particles of silica fume could clearly be observed, as shown in Figure 3a,c. The images of the as-prepared SF-SiC powder are shown in Figure 3b,d, which reveal that SF-SiC has porous and irregular particle morphologies. This is due to the large amount of heat released by magnesium thermal reaction, which seriously destroyed the morphology and structure of SF-SiO₂. At the same time, the thermal effect greatly improved the values of specific surface areas and average pore volumes of SF-SiC, and such results can also be seen in Table 2. The larger specific areas of SF-SiC support may provide more attachment sites for the active component. Compared with the amorphous silica fume (Figure 3e), the HRTEM image (Figure 3f) shows that the SF-SiC has good crystallinity with distinct lattice fringes of 0.251 nm and 0.262 nm corresponding to the SiC (102) and (101) planes, respectively.

In order to analyze and evaluate the distribution of Ni particles in the above catalysts, the SEM and HRTEM images of the freshly reduced catalysts Ni/SF-SiO₂ and Ni/SF-SiC are shown in Figure 4. It can be clearly observed that small Ni particles were dispersed over the Ni/SF-SiO₂ surface with aggregating phenomenon, as shown in Figure 4a. At the same time, the Ni particles can be clearly observed, which was caused by different contrast values in the images of Figure 4c,d. In comparison with Ni/SF-SiO₂ (mean sizes of Ni particles, 12.6 nm), the smaller Ni particles uniformly distributed in Ni/SF-SiC (mean sizes of Ni particles, 10.9 nm), it is obvious that Ni particles have better dispersion in Ni/SF-SiC than Ni/SF-SiO₂ [21,33,34]. The smaller Ni nanoparticles on Ni/SF-SiC could be attached to the stronger metal support interaction between Ni and SF-SiC, compared with Ni/SF-SiO₂ [35]. Moreover, the smaller Ni particles are beneficial for a high methanation rate. From Figure 4e,f, the lattice spacing of ca. 0.176 nm and 0.203 nm correspond to the Ni (200) and (111) plane. In Figure 4f, many distortions can be clearly observed, which were related to the novel defects-rich structure. Meanwhile, the defect-rich structure was also present in Ni/SF-SiO₂ catalysts (Figure 4e) [36]. The HRTEM element mapping of Ni/SF-SiO₂ and Ni/SF-SiC are shown in Figure 4 and it can be clearly observed that the larger Ni particles were dispersed on spherical morphology of SF-SiO₂ surface, but the smaller Ni nanoparticles were highly dispersed on the support of SF-SiC [37].

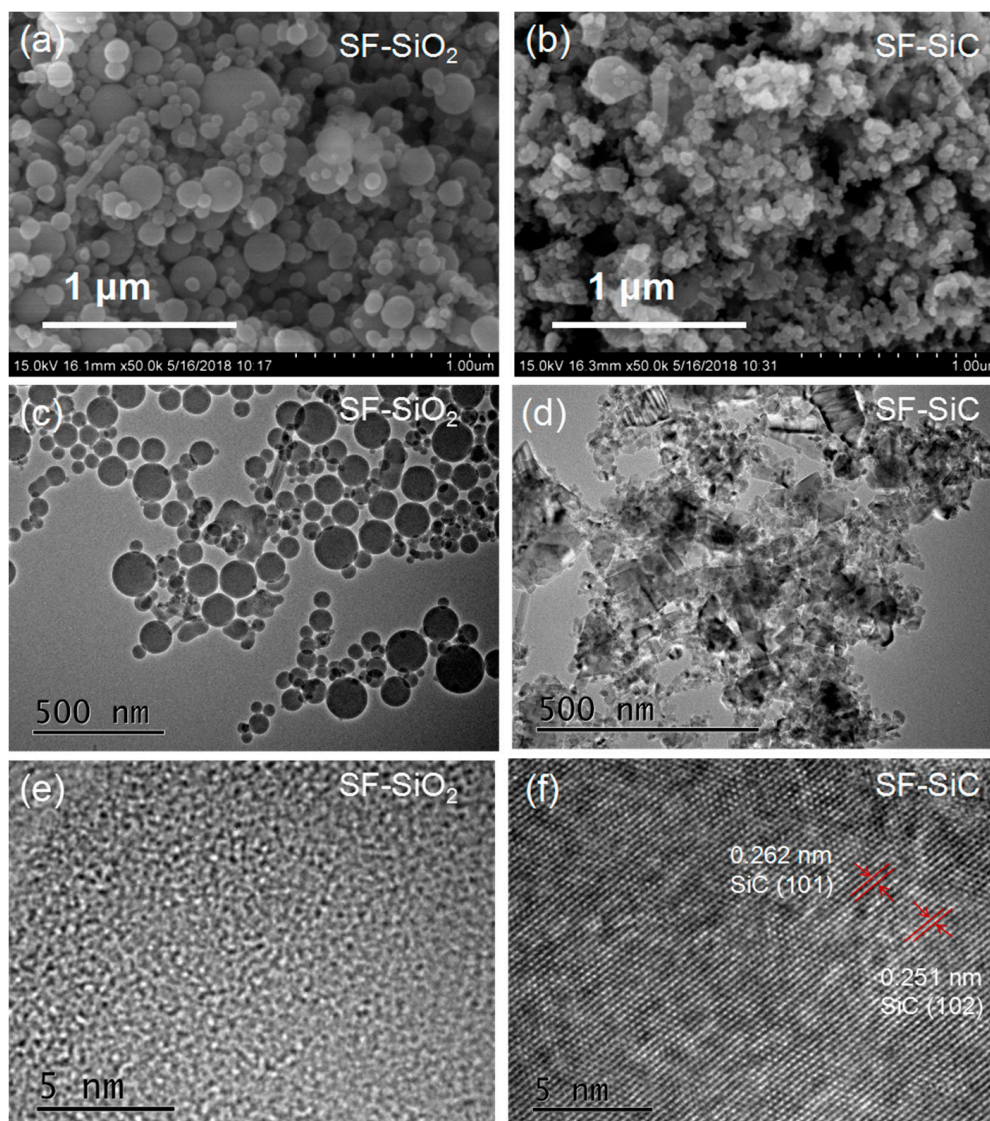


Figure 3. SEM images of the samples: (a) SF-SiO₂, (b) SF-SiC; HRTEM images of samples: (c,e) SF-SiO₂; (d,f) SF-SiC.

The N₂ adsorption–desorption was employed to measure the physical properties of the catalysts, as shown in Table 2. Compared with SF-SiO₂-support catalysts, the SF-SiC supporting catalysts show higher specific surface areas and pore volume, which should be attributed to the influence of molten salt-mediated magnesiothermic reduction [14]. Figure 3 shows that the surface of SiO₂ was smooth with a few pores. However, after loading Ni species, the specific surface areas and pore volume of Ni/SF-SiO₂ were obviously increased, which may be attributed to the rough surface of Ni/SF-SiO₂ produced by Ni particles loading and many holes produced among these Ni particles. However, the Ni precursors were introduced to the interior pore walls and the pore of the support was blocked, which explained that the specific surface areas and pore volume of Ni/SF-SiC were decreased. At the same time, this phenomenon also caused a slight change of average pore diameter in the Ni/SF-SiO₂ and Ni/SF-SiC catalysts [38].

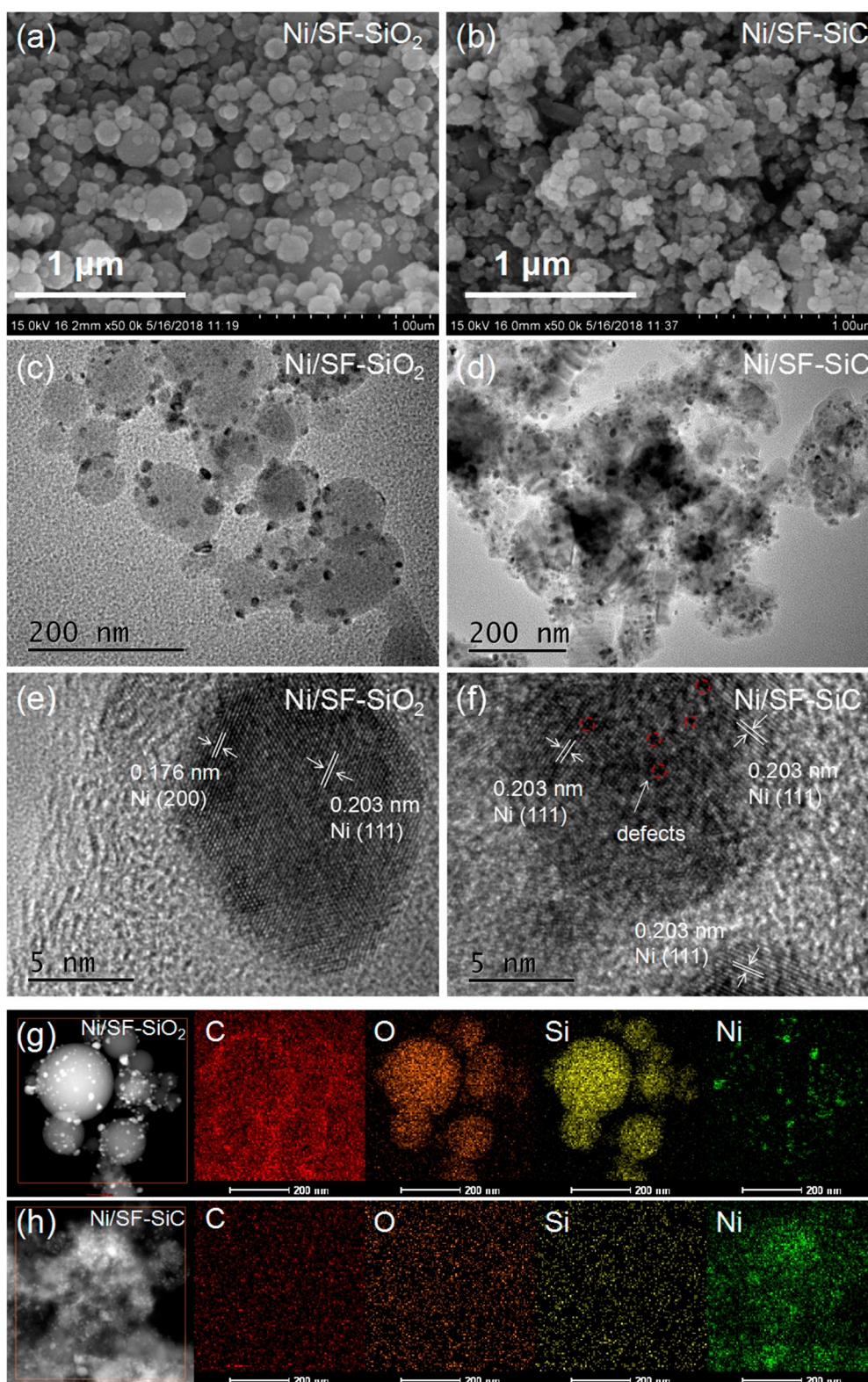


Figure 4. SEM images of the samples: (a) Ni/SF-SiO₂, (b) Ni/SF-SiC. HRTEM images of the reduced catalysts: (c,e) Ni/SF-SiO₂ and (d,f) Ni/SF-SiC. HRTEM elemental mapping images of C, O, Si and Ni of (g) Ni/SF-SiO₂ and (h) Ni/SF-SiC.

In Figure 5, based on the temperature programmed reduction (TPR) results, the curves of the two catalysts are similar. There was a strong peak with a shoulder peak in the NiO/SF-SiO₂,

the previous peak in the low temperature region was related to α -type NiO species and played a dominant role in nickel oxide species, which were assigned to the weaker interaction in Ni/SF-SiO₂ [31], and another peak was corresponded to β -type NiO species, which had a stronger interaction with the SF-SiO₂ [39,40]. In comparison with the NiO/SF-SiO₂ catalyst, the spectrum of the NiO/SF-SiC also had a broader peak, and the peak at a higher temperature could be associated with the reduction of nickel silicate, implying the enhanced interaction between NiO and the support of SF-SiC [33,41]. In addition, the overlapping peaks of TPR profiles were fitted by the Gaussian function and classified into four peaks; the peak positions and the quantitative results of relative content are shown in Table 3. It can be seen that there were four peaks in the NiO/SF-SiC. However, there were just three reduction peaks in NiO/SF-SiO₂, suggesting that the interaction between NiO and support was weaker. Compared with NiO/SF-SiO₂, the fraction of β -type NiO species of NiO/SF-SiC was larger, implying a stronger interaction between NiO and support. By comparing the H₂ consumption of the reduction peaks for the two catalysts, it can be found that more H₂ was consumed in the NiO/SF-SiC catalyst.

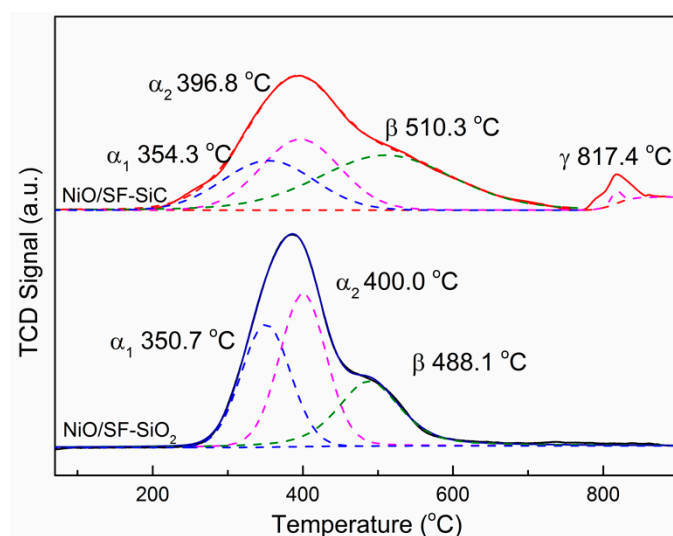


Figure 5. H₂-TPR profiles of the as-prepared NiO/SF-SiO₂ and NiO/SF-SiC catalysts.

Table 3. Gaussian fitting analysis of H₂ temperature programmed reduction (H₂-TPR) patterns of different catalysts.

Samples	Reduction Temperature (°C)				Relative Content (%)				H ₂ Consumption (mmol/g)			
	α_1	α_2	β	γ	α_1	α_2	β	γ	α_1	α_2	β	γ
NiO/SF-SiO ₂	350.7	400.0	488.1	–	32.9	40.5	26.6	–	0.46	0.56	0.37	–
NiO/SF-SiC	354.3	396.8	510.3	817.4	24.6	31.1	43.5	0.8	0.33	0.41	0.58	0.09

The two catalysts were characterized by the X-ray photoelectron spectroscopy (XPS), as illustrated in Figure 6. In Ni/SF-SiO₂, the Ni 2p_{3/2} binding energy (BE) of 852.91 eV was related to metallic Ni⁰, while the Ni 2p_{3/2} BE 856.78 eV with the satellite peak of 861.02 eV and the Ni 2p_{1/2} BE of 870.0 and 879.49 eV were assigned to Ni²⁺ species, which correspond to the partially oxidized nickel species. Compared with Ni/SF-SiO₂, the Ni 2p_{3/2} and 2p_{1/2} BEs (857.02, 861.50, 870.88 and 879.98 eV, respectively) of Ni²⁺ species of Ni/SF-SiC was improved. Furthermore, as for Ni/SF-SiO₂, the spectrum of the Ni 2p_{3/2} and 2p_{1/2} shown peaks at 855.24 and 873.26 eV, respectively, which could be ascribed to Ni³⁺ defects species [42,43]. However, the BE of Ni³⁺ species (855.50 and 873.78 eV) of Ni/SF-SiC was increased. The numerous Ni³⁺ in the two catalysts was generated from Ni and O vacancies in the process of calcination for forming the Ni_xO_y species. The surfaces of Ni²⁺ were oxidized to Ni³⁺ for forming charge neutrality around the Ni and O vacancies, and the surface Ni³⁺ active sites, which may facilitate charge-transfer and enhance CO and H₂ adsorption [42]. It is obvious

that Ni^{2+} and Ni^{3+} species were playing a dominate role in Ni/SF- SiO_2 and Ni/SF-SiC. Compared with Ni/SF- SiO_2 (852.91 eV), the binding energy of Ni^0 in Ni/SF-SiC (853.43 eV) was shifted to a higher binding energy, which is associated to the enhanced metal-support interactions between Ni and SF-SiC. From Table 4, there were about 5.2% of Ni elements on the Ni/SF-SiC surface, and that of Ni/SF- SiO_2 was 4.7%, which indicates that Ni was easily exposed to the surface of Ni/SF-SiC. In addition, the ratio of Ni^0/Ni and Ni^{3+}/Ni was about 11.2% and 31.0% for Ni/SF-SiC, respectively, which was higher than for Ni/SF- SiO_2 at 11.0% and 27.0%, demonstrating that the Ni species of Ni/SF-SiC were easily oxidized due to their good dispersion and smaller Ni nanoparticles, and there were more vacancies in Ni/SF-SiC.

In Figure 6b, the O 1s spectra of Ni/SF- SiO_2 and Ni/SF-SiC catalysts could be distinguished into four sub-peaks: The weakly binding energy peaks (O_I and O_{II}) were related to the surface lattice oxygen and the adsorbed oxygen [44], respectively; the higher binding energy (O_{III} and O_{IV}) corresponded to the defects with a low oxygen coordination and the metal-oxygen bonds, respectively [45]. The binding energy of O 1s of Ni/SF-SiC was higher than Ni/SF- SiO_2 , demonstrating that the stronger metal-support interactions between Ni and SF-SiC [21]. For the catalysts, the presence of Ni^{3+} and O_{III} could further promote the activity of reactive sites in methanation [45]. In Figure 6c, the Si 2p binding energy of 100.7 eV and 103.0 eV were attributed to the Si-C and Si-O bond in Ni/SF-SiC, respectively. There is only an Si-O bond in Ni/SF- SiO_2 [46]. In Figure 6d, the spectrum C 1s of Ni/SF-SiC (282.7, 285.0, 288.8 eV) corresponded to C-Si, C-C and C=O, respectively [47].

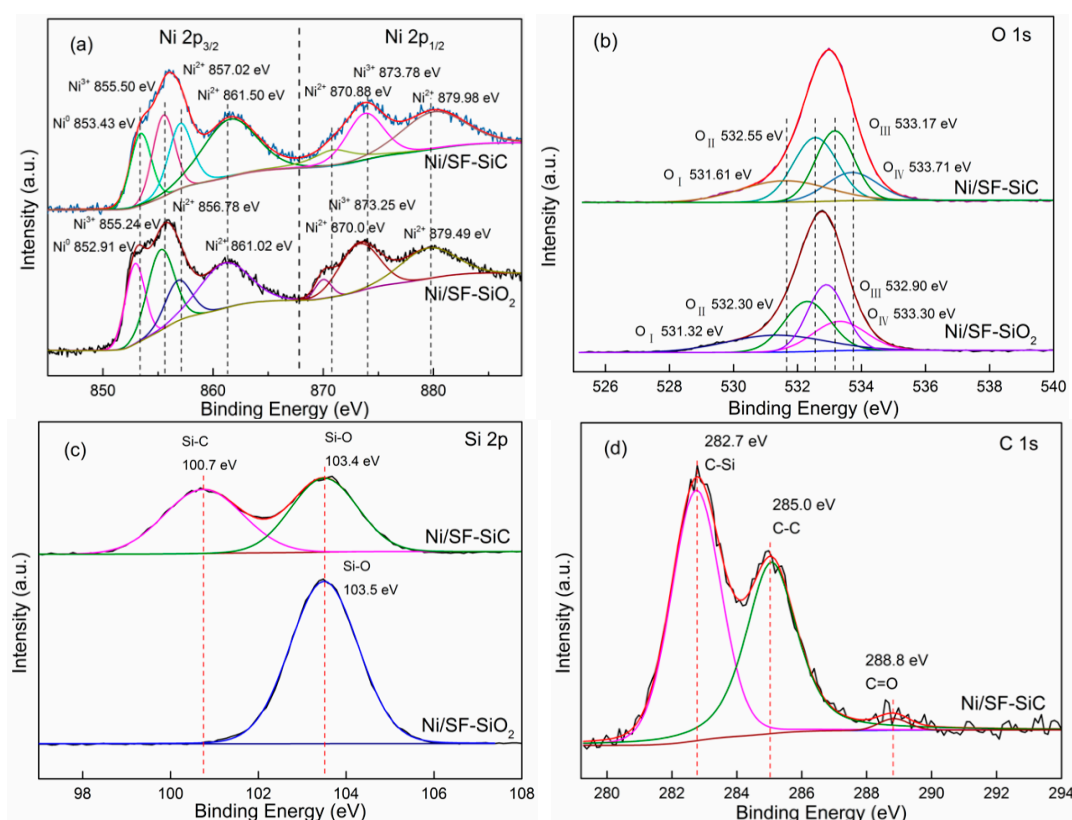


Figure 6. Ni 2p (a), O 1s (b), Si 2p (c) and C 1s (d) XPS spectra of the freshly reduced Ni/SF- SiO_2 and Ni/SF-SiC.

Table 4. Elemental analysis of Ni, O, Si, and C elements content by X-ray photoelectron spectroscopy (XPS).

Samples	Ni (%)	Ni^0/Ni (%)	Ni^{2+}/Ni (%)	Ni^{3+}/Ni (%)	O (%)	Si (%)	C (%)
Ni/SF- SiO_2	4.7	11.0	62.0	27.0	59.7	27.1	8.6
Ni/SF-SiC	5.2	11.2	57.8	31.0	44.2	30.5	20.1

The SEM and HRTEM images of the used Ni/SF-SiO₂ and used Ni/SF-SiC catalysts are shown in Figure 7. Compared with the freshly Ni/SF-SiO₂, Ni particles had some agglomeration in the used Ni/SF-SiO₂ (see Figure 3), and Ni particles of used Ni/SF-SiO₂ were larger than fresh Ni/SF-SiO₂ catalyst for the Ni particles migrated. Furthermore, the migration of Ni particles was caused by the weaker interaction between Ni species and SF-SiO₂. In contrast, Ni particles were still keeping good dispersion over the used Ni/SF-SiC, and the mean size of Ni particles in u-Ni/SF-SiO₂ and u-Ni/SF-SiC was 18.9 and 12.3 nm, respectively. In the Ni/SF-SiO₂ catalyst, the particles sizes of Ni species were larger, as compared with the freshly Ni/SF-SiO₂ (see Table 2). The Ni particles of Ni/SF-SiC catalysts always remained smaller, illustrating the stronger anti-sintering and higher Ni dispersion characteristics of Ni/SF-SiC than Ni/SF-SiO₂ [23].

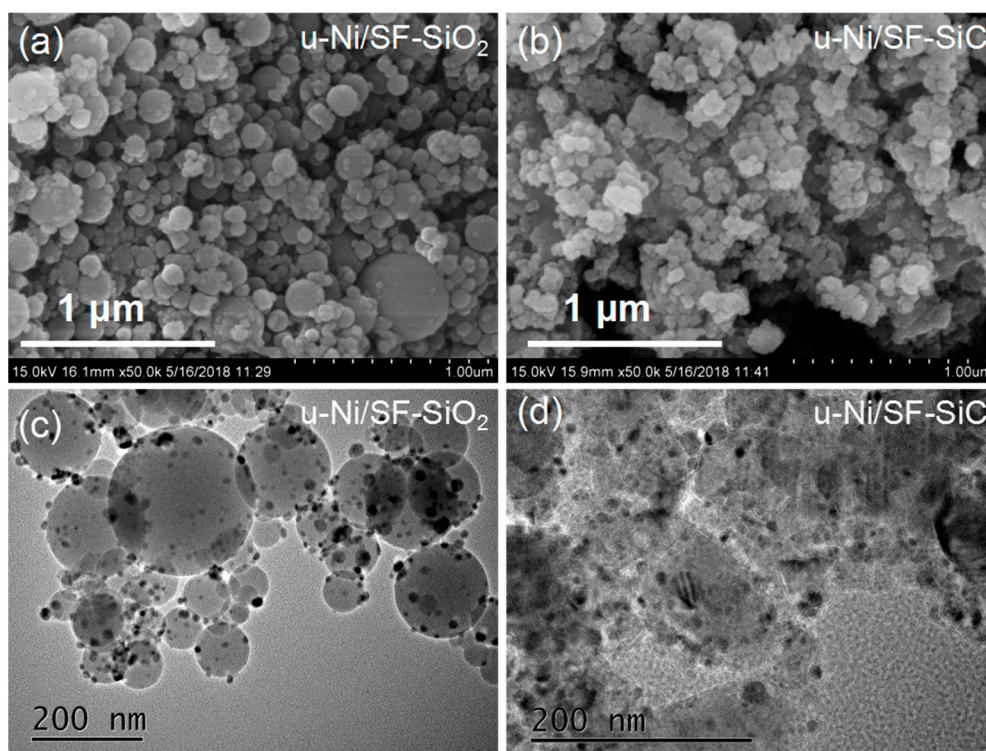


Figure 7. SEM images of the samples: (a) Used Ni/SF-SiO₂, (b) used Ni/SF-SiC. HRTEM images of (c) used Ni/SF-SiO₂ and (d) used Ni/SF-SiC.

The Vienna ab initio simulation package (VASP) was employed for the first-principles calculations [48,49]. The generalized gradient approximation was in the Perdew–Burke–Ernzerhof (PBE) form [50]. Chemisorption of CO and H₂ on the surface of catalyst to ensure that the C–O and H–H bonds were sufficiently activated is the necessary prerequisite to a high-performance methanation catalyst [51]. Therefore, the adsorption of CO and H₂ on Ni- and Ni_{vac}-based catalysts was investigated. Two stable adsorption configurations were taken into account, as shown in Figure 8. For the Ni–CO and Ni_{vac}–CO configuration, both two C atoms interact with metal atom, forming C–Ni bonds (Figure 8a,c). For the Ni–H₂ and Ni_{vac}–H₂ structure, only one Ni atom interact with two H atoms, forming Ni–H bonds (Figure 8b,d). From the above adsorption structure, the calculated binding energy (E_b) of CO and H₂ on defect-free Ni and Ni_{vac} are presented in Figure 8. The adsorption energy (absolute value) of CO and H₂ in Ni_{vac} was 1.84 and 4.88 eV respectively, which were significantly larger than that of CO and H₂ on defect-free Ni (1.83 and 4.76 eV, respectively), indicating that the vacancies in the Ni structure were more favorable for adsorbing CO and H₂ molecules [52,53]. Accordingly, the defect-rich Ni catalysts were superior to the defect-free Ni catalysts in the methanation.

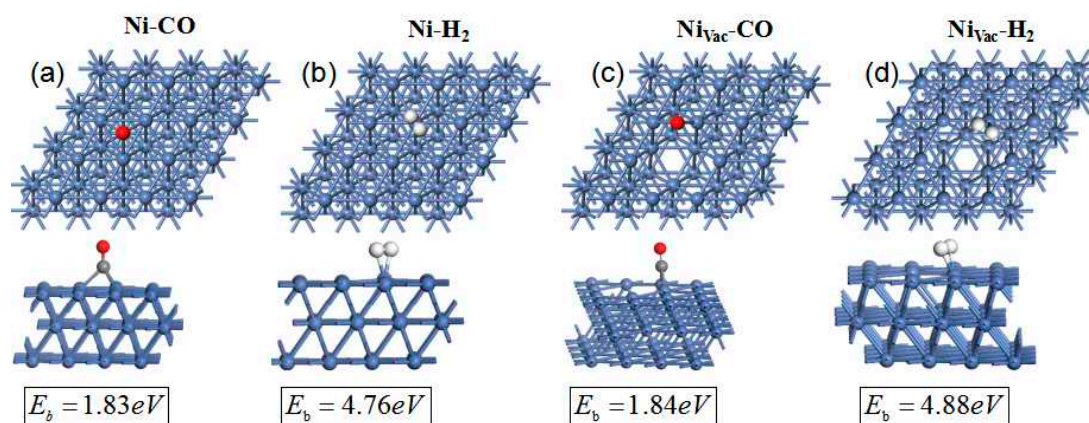


Figure 8. First-principles study of surface CO and H₂ adsorption on different sites. Top and side views of the structures of (a) Ni and (c) Ni vacancies with CO adsorption, (b) Ni, (d) Ni vacancies with H₂ adsorption. DFT-calculated adsorption energies (E_b) of CO and H₂ molecules on the surfaces of Ni and Ni vacancies are also presented, respectively. Blue, red, gray and white balls represent the Ni, O, C, and H atoms, respectively.

3. Materials and Methods

3.1. Preparation of Catalysts

The details for waste silica fume (Hesheng Silicon Industry Co., Ltd., Xinjiang, China) tested by X-ray fluorescence (XRF) were as follows: (wt %) SiO₂ 97.55, CaO 0.81, K₂O 0.43, Al₂O₃ 0.42, MgO 0.31, SiO₃ 0.12, Na₂O 0.11, Fe₂O₃ 0.08, P₂O₅ 0.06, and others 0.11. The waste silica fume (5 g) was mixed with 1.3 g of Acetylene black and 6.4 g Mg powder with 2.79 g NaCl and 3.56 g KCl, and transferred to a graphite boat. The mixture powders were calcined at a temperature of 1100 °C for 3 h in argon atmosphere. The heating rate from room temperature to 700 °C was 10 °C/min, and from 700 °C to 1100 °C was 5 °C/min. The resulting solid was exposed to 2 M aqueous HCl for 3 h to remove magnesium and magnesium oxide. The solution was subsequently filtered and washed repeatedly with water and then dried in an oven overnight at 100 °C. Additionally, the synthesized samples were heat-treated in air at 700 °C for 3 h to remove residual carbon. Moreover, in order to remove unreacted SiO₂, the product was immersed in the solution of NaOH and HF, respectively, and this was followed by washing thoroughly by repeated centrifugation. The final production was SF-SiC.

This work employed impregnation method to synthesize the catalysts: 2 g SF-SiC nano material was immersed in the aqueous solution of Ni(NO₃)₂·6H₂O (1.1235 g, Shanghai Macklin Biochemical Co., Ltd., Shanghai, China, AR, >98%) and stirred for 12 h at 80 °C, then dried for 12 h at 80 °C and calcined at 550 °C for 3 h at the rate of 10 °C/min [31]. The obtained catalyst was NiO/SF-SiC. The wasted silica fume was prepared into catalyst NiO/SF-SiO₂ in the same way.

3.2. Physical Characterization of the Synthesized Samples

The chemical composition of waste silica fume was analyzed by using X-ray fluorescence (XRF, XRF-1800). The powers were characterized by X-ray diffraction (XRD, Bruker D8 Advance X-ray diffractometer with Cu K α radiation ($\lambda = 1.5406 \text{ \AA}$) operated at 40 kv and 40 mA). H₂ temperature programmed reduction (H₂-TPR) was tested by AutoChemII2920 from room temperature to 900 °C at the rate of 10 °C/min with a gas (10 vol.% H₂/Ar) flow of 30 mL/min at 900 °C. The surface chemical composition was studied by an X-ray photoelectron spectroscopy (XPS) conducted on a Thermo Scientific Escalab 250Xi. The Micromeritics ASAP 2460 BET apparatus was used to measure the Brunauer–Ennett–Teller (BET) specific surface area and Barrett–Joyner–Halenda (BJH) pore structure of the catalysts. The microscopic feature of the catalysts was researched by field emission scanning electron microscope (SEM) (S-4800, Hitachi, Tokyo, Japan) and transmission electron microscopy (TEM)

(TecaiG2F20, FEI, 200 kV). Energy dispersed spectroscopy (EDS) (Tecnai G2 F20 S-TWIN (200 KV) was conducted to determine the elemental distribution.

3.3. CO Methanation Performance Test of Powdered Catalyst

The reactivity of the catalysts was tested in a fixed bed reactor (Tianjin Tianda Tianrui Petrochemical Equipment Manufacturing Co., Ltd., Tianjin, China.) at atmospheric pressure with a stainless steel tubular microreactor (a 66 cm long with an inner diameter of 10 mm). The 0.217 g catalyst was placed in the middle of the reaction tube, and before the feed syngas H₂/CO with a volume ratio of 3:1 was introduced to the reactor, the catalyst was reduced in 60 mL/min H₂ at 500 °C for 2 h. Then, the CO methanation performance tested in the temperature region of 250–550 °C at intervals of 50 °C, at a synthesis gas (Beijing AP BAIF Gases Industry CO., Ltd., Beijing, China.) flow rate of 65 mL/min and a weight space velocity of 18,000 mL·g⁻¹·h⁻¹. The composition of effluent gases was analyzed by gas chromatography (GC-2014C, SHIMADZU CO., Ltd., Beijing, China.) with TDX-01 column. We also conducted 50 h lifetime tests for Ni/SF-SiO₂ and Ni/VMT-SiC catalysts at 350 °C with all other parameters adopting the testing values. The CO conversion, CH₄ selectivity and yield are defined as follows:

$$\text{CO conversion: } X_{\text{CO}} (\%) = [\text{CO}]_{\text{in}} - [\text{CO}]_{\text{out}} / [\text{CO}]_{\text{in}} \times 100\% \quad (1)$$

$$\text{CH}_4 \text{ selectivity: } S_{\text{CH}_4} (\%) = [\text{CH}_4]_{\text{out}} / [\text{CO}]_{\text{in}} - [\text{CO}]_{\text{out}} \times 100\% \quad (2)$$

$$\text{CH}_4 \text{ yield: } Y_{\text{CH}_4} = [\text{CH}_4]_{\text{out}} / [\text{CO}]_{\text{in}} \times 100\% \quad (3)$$

Here, [CO]_{in} is the moles of CO in the feed stream, [CO]_{out} is the moles of CO in the effluent gas; [CH₄]_{out} is the moles of CH₄ in the effluent gas.

4. Conclusions

A large quantity of silica fume is deserted in industrial disposal with the development of the metallic silicon industry, which brings about resources wasting, and results in serious pollution by the dust and powder. In this work, silicon carbide ceramics were successfully synthesized using waste silica fume, and we prepared defect-rich Ni/SF-SiO₂ and Ni/SF-SiC catalysts by conventional impregnation method. The presence of Ni vacancies enhanced the adsorption energy of CO and H₂, which significantly improved the catalytic performance for methanation. Compared to the Ni/SF-SiO₂ counterpart, the Ni/SF-SiC catalyst exhibited a higher reactivity and stronger anti-sintering, which could be related to the excellent thermal conductivity of SF-SiC and the good dispersion and stronger metal-support interaction in the Ni/SF-SiC catalyst. Therefore, making full use of the “garbage” generated in the industrial production process, turning waste into treasure, not only achieves the maximum use of resources, but also makes a great contribution to the protection of the environment.

Author Contributions: F.Y., G.G. and J.Z. designed and administered the experiments; Q.S. performed experiments; Q.S., X.Z., J.L., X.R., H.Z., M.Z. and B.D. collected and analyzed data. All authors discussed the data and wrote the manuscript.

Funding: The research was funded by [Major Science and Technology Project of Xinjiang Bingtuan] grant number [2017AA007], [the National Natural Science Foundation of China] grant number [21403144, 11464038, 11764034], [the Program for Changjiang Scholars and Innovative Research Team in University] grant number [IRT_15R46].

Acknowledgments: The work was supported by Major Science and Technology Project of Xinjiang Bingtuan (No. 2017AA007), the National Natural Science Foundation of China (Grant Nos. 21403144, 11464038, 11764034), and the Program for Changjiang Scholars and Innovative Research Team in University (No. IRT_15R46).

Conflicts of Interest: The authors declare no conflict of interest.

References

1. Li, Q.; Wang, C.-A.; Tie, S. Synthesis of bamboo-like SiC whiskers from waste silica fume. *Cryst. Res. Technol.* **2014**, *49*, 290–297. [[CrossRef](#)]
2. Moen, M.; Halvorsen, T.; Mørk, K.; Velken, S. Recycling of silicon metal powder from industrial powder waste streams. *Met. Powder Rep.* **2017**, *72*, 182–187. [[CrossRef](#)]
3. Zhong, Y.; Shaw, L.L.; Manjarres, M.; Zawrah, M.F. Synthesis of Silicon Carbide Nanopowder Using Silica Fume. *J. Am. Ceram. Soc.* **2010**, *93*, 3159–3167. [[CrossRef](#)]
4. Danghyan, V.; Novoa, S.C.; Mukasyan, A.; Wolf, E.E. Pressure dilution, a new method to prepare a stable Ni/fumed silica catalyst for the dry reforming of methane. *Appl. Catal. B Environ.* **2018**, *234*, 178–186. [[CrossRef](#)]
5. Ji, H.; Huang, Z.; Chen, K.; Li, W.; Gao, Y.; Fang, M.; Liu, Y.G.; Wu, X. Synthesis of Si₃N₄ powder with tunable α/β -Si₃N₄ content from waste silica fume using carbothermal reduction nitridation. *Powder Technol.* **2014**, *252*, 51–55. [[CrossRef](#)]
6. Wang, Y.; Chen, J.; Lei, X.; Ren, Y.; Wu, J. Preparation of high silica microporous zeolite SSZ-13 using solid waste silica fume as silica source. *Adv. Powder Technol.* **2018**, *29*, 1112–1118. [[CrossRef](#)]
7. Kumar, P.; Mal, N.; Oumi, Y.; Yamana, K.; Sano, T. Mesoporous materials prepared using coal fly ash as the silicon and aluminium source. *J. Mater. Chem.* **2001**, *11*, 3285–3290. [[CrossRef](#)]
8. Zhang, T.; Hu, L.; Liang, J.; Han, Y.; Lu, Y.; Zhu, Y.; Qian, Y. Porous silicon nano-aggregate from silica fume as an anode for high-energy lithium-ion batteries. *RSC Adv.* **2016**, *6*, 30577–30581. [[CrossRef](#)]
9. Li, P.; Zhu, M.; Tian, Z.; Han, Y.; Zhang, Y.; Zhou, T.; Kang, L.; Dan, J.; Guo, X.; Yu, F.; et al. Two-Dimensional Layered Double Hydroxide Derived from Vermiculite Waste Water Supported Highly Dispersed Ni Nanoparticles for CO Methanation. *Catalysts* **2017**, *7*, 79. [[CrossRef](#)]
10. Li, P.; Yu, F.; Altaf, N.; Zhu, M.; Li, J.; Dai, B.; Wang, Q. Two-Dimensional Layered Double Hydroxides for Reactions of Methanation and Methane Reforming in C1 Chemistry. *Materials* **2018**, *11*, 221. [[CrossRef](#)]
11. Liu, Q.; Qiao, Y.; Tian, Y.; Gu, F.; Zhong, Z.; Su, F. Ordered Mesoporous Ni-Fe-Al Catalysts for CO Methanation with Enhanced Activity and Resistance to Deactivation. *Ind. Eng. Chem. Res.* **2017**, *56*, 9809–9820. [[CrossRef](#)]
12. Bian, Z.; Xin, Z.; Meng, X.; Tao, M.; Lv, Y.; Gu, J. Effect of Citric Acid on the Synthesis of CO Methanation Catalysts with High Activity and Excellent Stability. *Ind. Eng. Chem. Res.* **2017**, *56*, 2383–2392. [[CrossRef](#)]
13. Zhang, M.; Li, P.; Zhu, M.; Tian, Z.; Dan, J.; Li, J.; Dai, B.; Yu, F. Ultralow-weight loading Ni catalyst supported on two-dimensional vermiculite for carbon monoxide methanation. *Chin. J. Chem. Eng.* **2018**, *26*, 1873–1878. [[CrossRef](#)]
14. Tan, C.; Liu, J.; Zhang, H.; Wang, J.; Li, S.; Song, J.; Zhang, Y.; Zhang, S. Low temperature synthesis of 2H-SiC powders via molten-salt-mediated magnesiothermic reduction. *Ceram. Int.* **2017**, *43*, 2431–2437. [[CrossRef](#)]
15. Gao, P.-C.; Lei, Y.; Pérez, A.F.; Rajoua, K.; Zitoun, D.; Favier, F. New topotactic synthetic route to mesoporous silicon carbide. *J. Mater. Chem.* **2011**, *21*, 15798–15805. [[CrossRef](#)]
16. Wang, H.; Gao, S.; Peng, S.; Zhou, X.; Zhang, H.; Zhou, X.; Li, B. KD-S SiCf/SiC composites with BN interface fabricated by polymer infiltration and pyrolysis process. *J. Adv. Ceram.* **2018**, *7*, 169–177. [[CrossRef](#)]
17. Ma, Q.; Cai, L. Fabrication and oxidation resistance of mullite/yttrium silicate multilayer coatings on C/SiC composites. *J. Adv. Ceram.* **2017**, *6*, 360–367. [[CrossRef](#)]
18. Magnani, G.; Galvagno, S.; Sico, G.; Portofino, S.; Freda, C.; Burresi, E. Sintering and mechanical properties of β -SiC powder obtained from waste tires. *J. Adv. Ceram.* **2016**, *5*, 40–46. [[CrossRef](#)]
19. Fu, C.; Yang, Y.; Huang, Z.; Liu, G.; Zhang, H.; Jiang, F.; Wei, Y.; Jiao, Z. Investigation on the laser ablation of SiC ceramics using micro-Raman mapping technique. *J. Adv. Ceram.* **2016**, *5*, 253–261. [[CrossRef](#)]
20. Zhang, G.; Peng, J.; Sun, T.; Wang, S. Effects of the oxidation extent of the SiC surface on the performance of Ni/SiC methanation catalysts. *Chin. J. Catal.* **2013**, *34*, 1745–1755. [[CrossRef](#)]
21. Jin, G.; Gu, F.; Liu, Q.; Wang, X.; Jia, L.; Xu, G.; Zhong, Z.; Su, F. Highly stable Ni/SiC catalyst modified by Al₂O₃ for CO methanation reaction. *RSC Adv.* **2016**, *6*, 9631–9639. [[CrossRef](#)]
22. Yu, Y.; Jin, G.-Q.; Wang, Y.-Y.; Guo, X.-Y. Synthetic natural gas from CO hydrogenation over silicon carbide supported nickel catalysts. *Fuel Process. Technol.* **2011**, *92*, 2293–2298. [[CrossRef](#)]
23. Li, J.; Zhu, Q.; Peng, W.; Zhang, Q.; Luo, G.; Wei, F. Novel hierarchical Ni/MgO catalyst for highly efficient CO methanation in a fluidized bed reactor. *AIChE J.* **2017**, *63*, 2141–2152. [[CrossRef](#)]

24. Zhao, A.; Ying, W.; Zhang, H.; Ma, H.; Fang, D. Ni–Al₂O₃ catalysts prepared by solution combustion method for syngas methanation. *Catal. Commun.* **2012**, *17*, 34–38. [[CrossRef](#)]
25. Chen, D.; Christensen, K.; Ochoafernandez, E.; Yu, Z.; Totdal, B.; Latorre, N.; Monzon, A.; Holmen, A. Synthesis of carbon nanofibers: Effects of Ni crystal size during methane decomposition. *J. Catal.* **2005**, *229*, 82–96. [[CrossRef](#)]
26. Zhang, G.; Sun, T.; Peng, J.; Wang, S.; Wang, S. A comparison of Ni/SiC and Ni/Al₂O₃ catalyzed total methanation for production of synthetic natural gas. *Appl. Catal. A Gen.* **2013**, *462–463*, 75–81. [[CrossRef](#)]
27. Liu, Q.H.; Dong, X.F.; Lin, W.M. Highly selective CO methanation over amorphous Ni–Ru–B/ZrO₂ catalyst. *Chin. Chem. Lett.* **2009**, *20*, 889–892. [[CrossRef](#)]
28. Liu, S.-S.; Jin, Y.-Y.; Han, Y.; Zhao, J.; Ren, J. Highly stable and coking resistant Ce promoted Ni/SiC catalyst towards high temperature CO methanation. *Fuel Process. Technol.* **2018**, *177*, 266–274. [[CrossRef](#)]
29. Zhao, B.; Chen, Z.; Chen, Y.; Ma, X. Syngas methanation over Ni/SiO₂ catalyst prepared by ammonia-assisted impregnation. *Int. J. Hydrogen Energy* **2017**, *42*, 27073–27083. [[CrossRef](#)]
30. Tao, M.; Meng, X.; Lv, Y.; Bian, Z.; Xin, Z. Effect of impregnation solvent on Ni dispersion and catalytic properties of Ni/SBA-15 for CO methanation reaction. *Fuel* **2016**, *165*, 289–297. [[CrossRef](#)]
31. Li, P.; Zhu, M.; Dan, J.; Kang, L.; Lai, L.; Cai, X.; Zhang, J.; Yu, F.; Tian, Z.; Dai, B. Two-dimensional porous SiO₂ nanomesh supported high dispersed Ni nanoparticles for CO methanation. *Chem. Eng. J.* **2017**, *326*, 774–780. [[CrossRef](#)]
32. Gao, J.; Jia, C.; Li, J.; Zhang, M.; Gu, F.; Xu, G.; Zhong, Z.; Su, F. Ni/Al₂O₃ catalysts for CO methanation: Effect of Al₂O₃ supports calcined at different temperatures. *J. Energy Chem.* **2013**, *22*, 919–927. [[CrossRef](#)]
33. Li, P.; Wen, B.; Yu, F.; Zhu, M.; Guo, X.; Han, Y.; Kang, L.; Huang, X.; Dan, J.; Ouyang, F.; et al. High efficient nickel/vermiculite catalyst prepared via microwave irradiation-assisted synthesis for carbon monoxide methanation. *Fuel* **2016**, *171*, 263–269. [[CrossRef](#)]
34. Yu, Y.; Jin, G.; Wang, Y.; Guo, X. Synthesis of natural gas from CO methanation over SiC supported Ni–Co bimetallic catalysts. *Catal. Commun.* **2013**, *31*, 5–10. [[CrossRef](#)]
35. Yan, X.; Yuan, C.; Bao, J.; Li, S.; Qi, D.; Wang, Q.; Zhao, B.; Hu, T.; Fan, L.; Fan, B. Ni-based catalyst with enhanced Ni-support interaction for highly efficient CO methanation. *Catal. Sci. Technol.* **2018**, *8*, 3474–3483. [[CrossRef](#)]
36. Xie, J.; Zhang, H.; Li, S.; Wang, R.; Sun, X.; Zhou, M.; Zhou, J.; Lou, X.W.; Xie, Y. Defect-rich MoS₂ ultrathin nanosheets with additional active edge sites for enhanced electrocatalytic hydrogen evolution. *Adv. Mater.* **2013**, *25*, 5807–5813. [[CrossRef](#)] [[PubMed](#)]
37. Chen, X.; Jin, J.; Sha, G.; Li, C.; Zhang, B.; Su, D.; Williams, C.T.; Liang, C. Silicon–nickel intermetallic compounds supported on silica as a highly efficient catalyst for CO methanation. *Catal. Sci. Technol.* **2014**, *4*, 53–61. [[CrossRef](#)]
38. Lakshmanan, P.; Kim, M.S.; Park, E.D. A highly loaded Ni@SiO₂ core–shell catalyst for CO methanation. *Appl. Catal. A Gen.* **2016**, *513*, 98–105. [[CrossRef](#)]
39. Zhang, M.; Li, P.; Tian, Z.; Zhu, M.; Wang, F.; Li, J.; Dai, B.; Yu, F.; Qiu, H.; Gao, H. Clarification of Active Sites at Interfaces between Silica Support and Nickel Active Components for Carbon Monoxide Methanation. *Catalysts* **2018**, *8*, 293. [[CrossRef](#)]
40. Cai, W.-J.; Qian, L.-P.; Yue, B.; He, H.-Y. Rh doping effect on coking resistance of Ni/SBA-15 catalysts in dry reforming of methane. *Chin. Chem. Lett.* **2014**, *25*, 1411–1415. [[CrossRef](#)]
41. García-Vargas, J.M.; Valverde, J.L.; de Lucas-Consuegra, A.; Gómez-Monedero, B.; Sánchez, P.; Dorado, F. Precursor influence and catalytic behaviour of Ni/CeO₂ and Ni/SiC catalysts for the tri-reforming process. *Appl. Catal. A Gen.* **2012**, *431–432*, 49–56.
42. Zhao, Y.; Jia, X.; Chen, G.; Shang, L.; Waterhouse, G.I.; Wu, L.Z.; Tung, C.H.; O'Hare, D.; Zhang, T. Ultrafine NiO Nanosheets Stabilized by TiO₂ from Monolayer NiTi-LDH Precursors: An Active Water Oxidation Electrocatalyst. *J. Am. Chem. Soc.* **2016**, *138*, 6517–6524. [[CrossRef](#)]
43. Sasi, B.; Gopchandran, K.G. Nanostructured mesoporous nickel oxide thin films. *Nanotechnology* **2007**, *18*, 115613. [[CrossRef](#)]
44. Zhang, M.; Yu, F.; Li, J.; Chen, K.; Yao, Y.; Li, P.; Zhu, M.; Shi, Y.; Wang, Q.; Guo, X. High CO Methanation Performance of Two-Dimensional Ni/MgAl Layered Double Oxide with Enhanced Oxygen Vacancies via Flash Nanoprecipitation. *Catalysts* **2018**, *8*, 363. [[CrossRef](#)]

45. Wang, Y.; Xie, C.; Zhang, Z.; Liu, D.; Chen, R.; Wang, S. In Situ Exfoliated, N-Doped, and Edge-Rich Ultrathin Layered Double Hydroxides Nanosheets for Oxygen Evolution Reaction. *Adv. Funct. Mater.* **2018**, *28*, 1703363. [[CrossRef](#)]
46. Adhikari, S.; Eswar, N.K.; Sangita, S.; Sarkar, D.; Madras, G. Investigation of nano Ag-decorated SiC particles for photoelectrocatalytic dye degradation and bacterial inactivation. *J. Photochem. Photobiol. A Chem.* **2018**, *357*, 118–131. [[CrossRef](#)]
47. Hao, J.-Y.; Wang, Y.-Y.; Tong, X.-L.; Jin, G.-Q.; Guo, X.-Y. Photocatalytic hydrogen production over modified SiC nanowires under visible light irradiation. *Int. J. Hydrogen Energy* **2012**, *37*, 15038–15044. [[CrossRef](#)]
48. Kresse, G.; Furthmüller, J. Efficient iterative schemes for ab initio total-energy calculations using a plane-wave basis set. *Phys. Rev. B Condens. Matter* **1996**, *54*, 11169–11186. [[CrossRef](#)]
49. Kresse, G.; Furthmüller, J. Efficiency of ab-initio total energy calculations for metals and semiconductors using a plane-wave basis set. *Comp. Mater. Sci.* **1996**, *6*, 15–50. [[CrossRef](#)]
50. Perdew, J.P.; Burke, K.; Ernzerhof, M. Generalized Gradient Approximation Made Simple. *Phys. Rev. Lett.* **1998**, *77*, 3865–3868. [[CrossRef](#)]
51. Ling, C.; Bai, X.; Ouyang, Y.; Du, A.; Wang, J. Single Molybdenum Atom Anchored on N-Doped Carbon as a Promising Electrocatalyst for Nitrogen Reduction into Ammonia at Ambient Conditions. *J. Phys. Chem. C* **2018**, *122*, 16842–16847. [[CrossRef](#)]
52. Liu, Y.; Cheng, H.; Lyu, M.; Fan, S.; Liu, Q.; Zhang, W.; Zhi, Y.; Wang, C.; Xiao, C.; Wei, S.; et al. Low overpotential in vacancy-rich ultrathin CoSe₂ nanosheets for water oxidation. *J. Am. Chem. Soc.* **2014**, *136*, 15670–15675. [[CrossRef](#)] [[PubMed](#)]
53. Yan, D.; Li, Y.; Huo, J.; Chen, R.; Dai, L.; Wang, S. Defect Chemistry of Nonprecious-Metal Electrocatalysts for Oxygen Reactions. *Adv. Mater.* **2017**, *29*, 1606459. [[CrossRef](#)] [[PubMed](#)]



© 2019 by the authors. Licensee MDPI, Basel, Switzerland. This article is an open access article distributed under the terms and conditions of the Creative Commons Attribution (CC BY) license (<http://creativecommons.org/licenses/by/4.0/>).